Nigerian Journal of Technology (NIJOTECH)
Vol. 32, No. 1, March, 2013, pp. 117–122.
 ISSN 1115-8443

EFFECTS OF SINTERING TEMPERATURE ON THE DENSITY AND POROSITY OF SODIUM CHLORIDE PREFORMS FOR OPEN CELLED ALUMINIUM FOAM MANUFACTURING

R.E. Njoku[a], **A.R. Kennedy**[b]

Department of Mechanical, Materials and Manufacturing Engineering, University of Nottingham, UK.
Emails: [a] *romanus.njoku@unn.edu.ng;* [b] *andrew.kennedy@nottingham.ac.uk*

Abstract

Effects of sintering temperature on the density and porosity of sodium chloride preforms for aluminium foam manufacturing have been investigated. Cold pressed salt preforms were sintered at 730℃, 760℃ and 790℃ and different times ranging between 6- 18 hours in a carbolite furnace at a heating rate of 5℃/minute. The Results of density and porosity measurements show that the density and porosity of the preform can be varied by changing the sintering temperatures of the preforms. It was observed that the density of the preforms increases with sintering temperature at constant time and pre-sintering pressure while porosity has an inverse relationship with temperature. Results of scanning electron microscopic analyses, show sintering connection (bonding) between the salt beads at all the temperatures in which sintering was performed. Sintering of the sodium chloride perform was attributed to grain boundary diffusion and evaporation condensation mechanisms.

Keywords: sintering, preform, density, porosity, aluminium foam

1. Introduction

The sintering process has been an important operation in the fabrication of various materials into useful articles. Sodium chloride powders have long been used as a model system for the investigation of ceramic sintering behavior [1, 2]. However, the system is also interesting from a practical point of view because sintered sodium chloride preforms are used in the manufacture of highly porous metal foams by the replication process.

Metal foams are a new, as yet imperfectly-characterized, class of materials with low densities and novel physical, mechanical, thermal, electrical and acoustic properties [3]. They uniquely combine the properties of metals and those of porous cellular materials and offer potential for light-weight structures, for energy absorption, for thermal management and for acoustic absorption. The metal foam consists in structure that encloses open cells- randomly oriented and mostly homogeneous in size and shape. Most commercially available metal foams are based on aluminium, copper, nickel and metal alloys [4]. Metal foams have considerable applications in multifunctional heat exchangers, cryogenics, combustion chambers, cladding on buildings, strain isolation, buffer between a stiff structure and a fluctuating temperature field, geothermal operations, petroleum reservoirs, catalytic beds, compact heat exchangers for air borne equipment, air cooled condensers and compact heat sink for power electronics [3, 4].

Open-cell metal foams present high surface area to volume ratio as well as enhanced flow mixing and attractive stiffness and strength [4]. The most characteristic parameters of open-celled metal foam are the pore size, the pore density (the number of pores per linear inch), the porosity (defined as the volume of void divided by the total volume of foam) and relative density (defined as the density of foam divided by the density of metal) [5]. The overwhelming majority of metal foams in the market are closed-cell aluminium foam manufactured by liquid or semi-liquid foaming technologies [6]. These techniques are more suitable for producing closed-cell metallic foams which are basically used in structural applications. For functional applications such as sound absorption, heat dissipation and catalyst support, the open-cell foams are more desirable and are easily produced using the replication processes namely: sintering dissolution process-

Table 1: Effects of temperature on linear dimensions, mass and density of NaCl beads cold pressed at 50MPa and sintered for 12 hours. (N/B 1 & 2 denote measurements-before and after sintering, $d_1 = 2.23$cm).

TEMP (℃)	h_1 (cm)	V_1 (cm^3)	M_1 (g)	ρ_1 (g/cm^3)	d_2 (cm)	h_2 (cm)	V_2 (cm^3)	M_2 (g)	ρ_2 (g/cm^3)
790	2.62	10.23	14.98	1.46	2.05	2.38	7.86	12.47	1.59
760	2.62	10.23	14.98	1.46	2.07	2.42	8.14	12.73	1.56
730	2.63	10.27	15.01	1.46	2.08	2.43	8.26	12.81	1.55

Table 2: Effects of temperature on linear dimensions, mass and density of NaCl beads cold pressed at 40MPa and sintered for 12 hours. (N/B 1 & 2 denote measurements-before and after sintering, $d_1 = 2.23$cm).

TEMP (℃)	h_1 (cm)	V_1 (cm^3)	M_1 (g)	ρ_1 (g/cm^3)	d_2 (cm)	h_2 (cm)	V_2 (cm^3)	M_2 (g)	ρ_2 (g/cm^3)
790	2.91	11.37	14.95	1.31	2.06	2.63	8.77	12.61	1.44
760	2.90	11.32	14.94	1.32	2.08	2.68	9.11	12.82	1.41
730	2.91	11.37	14.95	1.31	2.08	2.67	9.07	12.64	1.39

ing or liquid infiltration method. The advantages of these methods are that the morphologies of the pores and their sizes are determined by the characteristics of the space holder particles and the foam porosity can easily be controlled by varying the metal/space holder volume ratio [1,7]. The production of open cell foam by infiltration processing involves four steps: preparation of leachable preform (usually from NaCl); Infiltration of molten metal into preform; Solidification of liquid metal; and dissolution of preform in a solvent or water. The microstructure of the resulting foam is controlled by the microstructure of the preform and their mechanical characteristics are consistent and reproducible [8].

Zhao et al [9] reported that the porosity of the as-manufactured foam is determined by the density of the prepared compact of the sodium chloride (NaCl) powder in the liquid infiltration process. The density of preform in turn, varies with sintering temperature. In order to vary the porosity of aluminium foams and thus increase their versatility, an understanding of the variation of density of compact sodium chloride (preform) at different sintering temperatures is very imperative.

Hence the aim of this paper is to critically investigate the effects of sintering temperature on the density and porosity of salt bead preforms used in the liquid infiltration of aluminium for open cell foam manufacturing.

2. Sintering Mechanism

Sintering occurs by atomic diffusion processes that are stimulated by high temperatures. This phenomenon causes substantial particle re-arrangement and consolidation especially in loosely packed bodies [10]. Okuyama [11] defined sintering as an irreversible thermodynamic phenomenon to convert unstable packed powder having excess free energy to stable agglomerates. During sintering, the atoms in the powder particles diffuse across the boundaries of the particles, fusing the particles together and creating one solid piece. Sintering phenomenon involves fusion of particles, volume reduction, decrease in porosity and increase in grain size. Amorphous materials sinter by viscous flow while polycrystalline materials sinter by one or more mechanisms occurring singly or in parallel depending on the materials system and the sintering conditions. The mechanisms include [12]: surface diffusion of atoms; evaporation/condensation of atoms; grain boundary diffusion and plastic deformation.

In general bulk transport mechanisms such as volume diffusion, grain boundary diffusion, plastic flow and viscous flow result in shrinkage or densification while surface transport does not. However, surface transport is important in inter-particle neck growth and the sintering of some covalent solids and low-stability ceramics. The entire sintering process is generally considered to occur in three stages [13, 14]: (i) initial stage, (ii) intermediate stage and (iii) the final stage. There is no clear cut distinction between the stages since the processes that are associated with each stage tend to overlap each other. The initial stage is characterized by particles re-arrangement, formation and growth of neck by diffusion (lattice or grain boundary), vapour transport, plastic flow, or viscous flow. Intermediate stage is considered to begin when the pores have attained their equilibrium shapes as dictated by surface and interfacial energies. In the final stage, isolated pores are eliminated and there is grain growth. The driving force for all these mechanisms is the tendency for the material to reduce its chemical potential or energy and this is accomplished by material transport from regions of high chemical potential to regions of lower chemical potential.

Coble [15], derived equations for estimating the rate of densification for lattice and grain boundary diffusion as follows:

Table 3: Effects of temperature on linear dimensions, mass and density of NaCl beads cold pressed at 30MPa and sintered for 12 hours. (N/B 1 & 2 denote measurements-before and after sintering, $d_1 = 2.23$cm).

TEMP (℃)	h_1 (cm)	V_1 (cm^3)	M_1 (g)	ρ_1 (g/cm^3)	d_2 (cm)	h_2 (cm)	V_2 (cm^3)	M_2 (g)	ρ_2 (g/cm^3)
790	3.15	12.30	14.57	1.18	2.08	2.92	9.98	12.77	1.28
760	3.15	12.30	14.57	1.18	2.08	2.93	9.96	12.37	1.24
730	3.15	12.30	14.57	1.18	2.13	2.97	10.58	12.81	1.21

Table 4: Effects of time on linear dimensions, mass and density of NaCl beads cold pressed at 50MPa and sintered at 760℃. (N/B 1 & 2 denote measurements-before and after sintering, $d_1 = 2.23$cm).

TIME (Hour)	h_1 (cm)	V_1 (cm^3)	M_1 (g)	ρ_1 (g/cm^3)	d_2 (cm)	h_2 (cm)	V_2 (cm^3)	M_2 (g)	ρ_2 (g/cm^3)
6	2.62	10.23	14.98	1.46	2.08	2.43	8.26	12.81	1.55
12	2.62	10.23	14.98	1.46	2.07	2.42	8.14	12.73	1.56
16.65	2.60	10.15	14.95	1.47	2.06	2.38	7.93	12.61	1.59

Lattice diffusion:

$$\frac{1}{\rho}\frac{d\rho}{dt} \approx \frac{AD_l\gamma_{sv}\Omega}{\rho G^3 KT} \tag{1}$$

Grain boundary diffusion:

$$\frac{1}{\rho}\frac{d\rho}{dt} \approx \frac{4}{3}\left(\frac{D_b\delta_b\gamma_{sv}\Omega}{G^4 KT\rho(1-\rho)^{\frac{1}{2}}}\right) \tag{2}$$

Where ρ is density of material, A is a constant, D_l and D_b are diffusion coefficients for lattice and grain boundary diffusion, γ_{sv} is specific surface energy, Ω is atomic volume, G is grain size, K is Boltzmann's constant, δ_b is grain boundary thickness, t is sintering tome and T is absolute temperature.

Ashby [16], gave the following equation for the rate of sintering by grain boundary diffusion mechanism as stated in equation 3 below:

$$\frac{d\Delta}{dt} = \frac{129\delta_b D_b\gamma_s\Omega}{KTa^4}\frac{\Delta^2(2\Delta-\Delta_0)}{\Delta-\Delta_0} \tag{3}$$

Where, Δ is the relative compact density at time t, Δ_0 is the initial relative compact density ($\Delta = \rho/\rho_0$ and $\Delta_0 = \rho_i/\rho_0$ where ρ is the powder compact density after sintering, ρ_i is the initial compact density and ρ_0 is the density of the non-porous material), a is the initial particle radius.

3. Experimentals

3.1. Production of sodium chloride preforms

15g of sodium chloride (with average particle size of 53μ) beads, produced according to procedure described in [17] were poured into a stainless steel die (⌀22.3mm), and pressures of 30, 40 and 50MPa were applied to compact the beads using a mechanical press. Green preforms were, thereafter, forced out of the die and preliminary measurements of mass and linear dimensions were made using an electronic balance and venier caliper respectively. The preforms were sintered in a carbolite furnace at 730℃, 760℃ and 790℃ for 6 and 12 hours. Some preforms were, however, sintered at 760℃ for 6, 12 and 16.65 hours. The furnace was programmed to operate at 5℃Min. The samples were re-measured after sintering. Each of the experiments was repeated three times.

3.2. X-ray micro computed tomography analysis

Salt preform samples were placed in a ⌀30mm container and rotated through 360° in a micro X-ray computed tomography (Scanco AG μCT 40) equipment. 2D images of the performs were obtained using medium resolution and threshold value of 260. The test revealed the variation of porosity across the microstructure of the samples.

3.3. Scanning electron microscopy analysis

The microstructure of the salt bead preforms was examined in a scanning electron microscope (SEM, Philips XL30) using a voltage of 15 KV and current density of 50μA. The samples were mounted on specimen holder using carbon cement and coated with platinum.

4. Results and Discussion

4.1. Density of preforms

The observed effects of temperature on linear dimensions, masses and densities of 1.0-1.4 mm sodium chloride beads (with 53 mean NaCl particle sizes), cold pressed at 50, 40, 30MPa respectively and sintered for 12 hours are shown in Tables 1-3. Table 4 shows the effect of time on the response of the salt bead samples to sintering at 760oC.

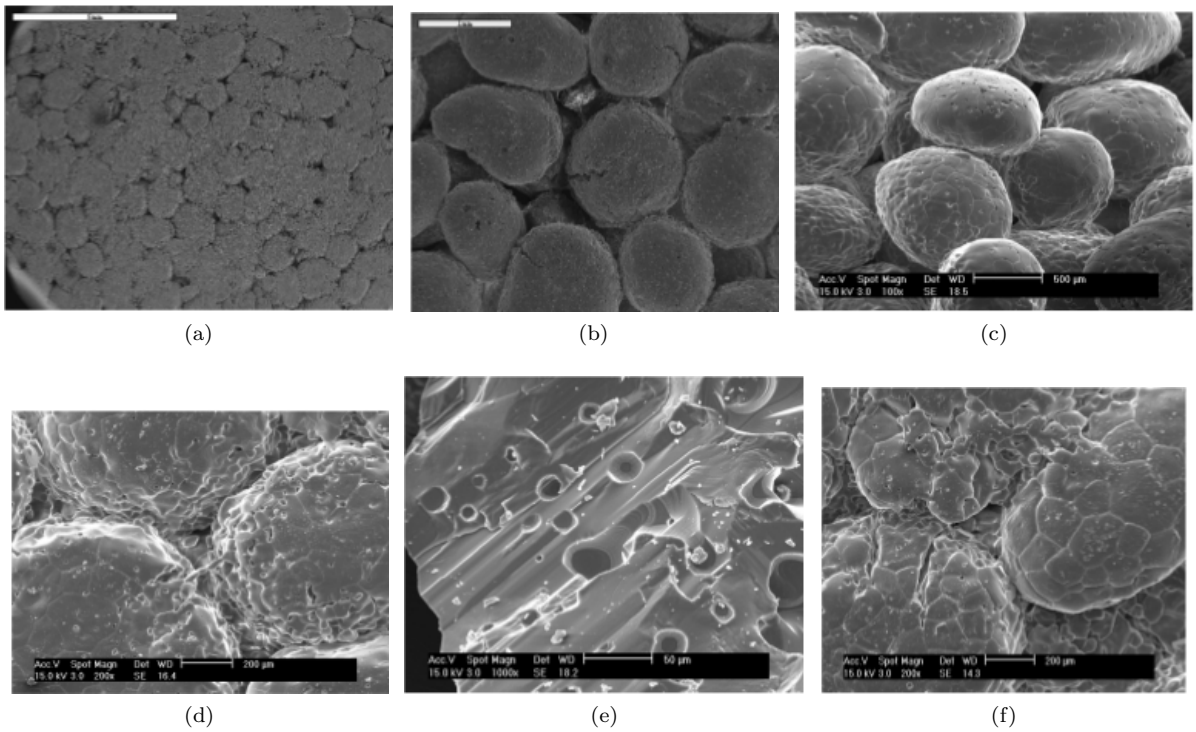

Figure 1: Scanning electron microscope images of NaCl salt beads (a) in green condition (b) 30MPa, 760℃ - 12h (c) loose beads, 760℃ (d) 40MPa, 760℃ - 12h (e) Fractured bead, 760℃ - 12h. (f) 40MPa, 790℃ - 12h.

It can be deduced from Tables 1-3 that the density of the salt bead preform can be varied between 1.21-1.59g/cm^3 – giving space holders with packing fraction that ranges from 57% to 75%. (Density of the salt bead was found from mercury porosimetry test to be 2.11g/cm^3). Thus the porosity of the preforms and hence some properties (permeability, convective heat transfer coefficient, and energy absorption capacity) of metal foams produced by liquid infiltration of these salt bead preforms can be varied and tailored to suit specific applications. It can also be deduced from these tables that densification occurred in the preforms at all the temperatures. Table 4 shows that there is no remarkable change in the density of the preforms sintered for 6 hours and 12 hours for salt beads pressed at a pressure of 50MPa and sintered at 760℃. Experimental results show that densification occurred in the sodium chloride preforms in all the sintering temperatures and forming conditions (cold-pressing at 30-50MPa) and that densification increases with forming pressure and sintering temperature. This is consistent with the findings of Gaillard et al [1] and Goodall et al [2].

Goodall et al [2], applying the Asby's and Swinkles' [16] conditions for rate determining mechanisms for sintering, suggested that sintering of sodium chloride, at the sintering temperature under consideration, occurs via two of the mechanisms stated in [12]. The mechanisms are: (i) grain boundary diffusion from grain boundary sources, which will lead to densification, and (ii) evaporation-condensation, which leads to neck growth without densification. Sintering of sodium chloride preform could be attributed to an inter-play of these two mechanisms. Grain boundary diffusion will initially dominate for all temperatures and past this initial stage, however, boundary diffusion-driven densification does not always remain dominant. Densification then stops because evaporation- condensation reduces significantly the neck curvature and in turn reduces the driving force for grain boundary diffusion [14].

4.2. Microstructural analysis

The micrographs of NaCl bead preforms in both green and sintered conditions are shown in figures 1 (a-f).

Figure 1a shows the micrograph of sodium chloride preform in green condition while Figure 1b shows the image of preform compacted at 30MPa and sintered at 760℃ for 12 hours. In Figures 1c and 1d, the SEM images of loose (non- compacted) salt beads, sintered at 760℃ for 12 hours and beads formed with applied pressure of 40MPa and sintered at 760℃ for 12 hours are shown respectively. In Figures 1e and 1f the micrographs of a fractured bead- sintered at 760℃ for 12 hours and that of preform, compacted with pressure of 40MPa and sintered at 790℃ for 12 hours are respectively shown. A critical examination of figures 1b

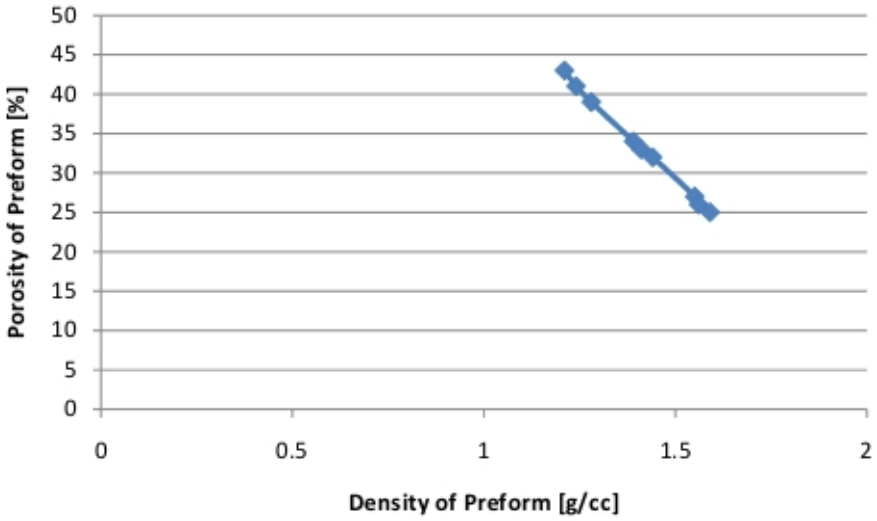

Figure 2: Variation of porosity with density of preform.

and 1d (preforms sintered at 760℃ for 12 hours) shows that the preform compacted with a higher pressure of 40MPa exhibited a higher degree of inter-bead bonding as evidenced by the growth of neck in between the beads while in the preform compacted with a lower pressure of 30MPa, there are gaps between beads and no visible necking. The preform compacted with the pressure of 40MPa and sintered at 790℃ for 12 hours (figure 1f) showed the formation and growth of inter-bead neck. This is probably due to the fact higher pressure increases the contact between beads and facilitates bulk transport across these beads [19]. Bonding between sodium chloride beads at the temperatures (730-790℃) under which the preforms were sintered could be attributed to grain boundary diffusion and evaporation-condensation mechanism [15]. Elongation of sodium chloride grains and preform beads can also be noticed for preforms compressed at 40MPa and sintered at 790℃ for 12 hours (figure 1f), suggesting grain growth and indicating stage III sintering operation [11,12]. Figure 1e is a magnified view of a fractured NaCl bead, sintered at 760℃ for 12 hours. It reveals the presence of pores within the sodium chloride grains which are probably due to gases generated during the decomposition of the binder material (glutinous rice) at 500℃ some of which might have been entrapped within the sodium chloride matrix.

4.3. Porosity of preform

The porosity (ε) of a preform is an indication of its volume fraction that is available for metal to occupy in the liquid infiltration processing of aluminium foams. Porosity was calculated from the formula [18],

$$\varepsilon\% = \frac{\rho_p}{\rho_b} \tag{4}$$

where ρ represents density and the subscripts p and b represent preform and bead particle respectively. The graph of the variation of porosity of preforms with density at all the sintering conditions investigated is shown in figure 2.

As shown in figure 2, porosity of the preforms varies inversely with density. The preform is a negative replica of the metal foam (the void fraction ε, of preform is a measure of the solid fraction of the metal foam). In general high porosity preforms give rise to dense metal foams while low porosity ones produce highly permeable open-celled metallic foams for functional applications such as thermal management and energy absorption.

Figure 3 shows the 2D images of x-ray micro computed tomography tests of sodium chloride preforms with 25%, 32% and 43% porosities, corresponding to preforms produced under conditions and scanning electron microscopic images shown in figures 1f, 1d and 1b, respectively. Figures 3a-c show that the number of interconnected pores in the preform increases as the porosity of the samples is increased. The specimen with 43% porosity (sintered at 730℃) had the largest number of interconnected pores and these pores are spaces for liquid metal to occupy during infiltration processing of aluminium foam.

(a)25% porosity (790℃) (b)32% porosity (760℃) (c)43% porosity (730℃). Figure 3: X-ray micro computer tomography images showing varying degrees of porosities in sodium chloride preforms sintered at different conditions.

5. Conclusion

The effects of sintering on the density and porosity of sodium preform were investigated. The study

of the sintering behavior of compacted sodium chloride beads is particularly of a practical importance because of its use in the manufacturing of highly porous cellular metals by replication method. The following inferences can be made from the results of this study:

- Application of pressure during compaction of sodium chloride beads increases the contact between the bead particles and enhances transport of materials across boundaries, leading to bonding between the salt beads;
- Sintering of sodium chloride preforms increases the density of the compacted salt beads within a reasonable range;
- Porosity increases inversely with the density of preform.

References

1. Gaillard, C., Despois, J.F. and Mortensen, A. Processing of NaCl Powders of Controlled Size and Shape for the Microstructural tailoring of Aluminium Foam. *Materials Science and Engineering*, Vol. 37, 2004, pp.250-262.
2. Goodall, R., Despois, J.F. and Mortensen, A. Sintering of NaCl Powder-Mechanisms and First Stage Kinetics. *Journal of European Ceramic Society*, Vol. 26, 2006, pp.3487-3497.
3. Banhart, J., Asby, M.F. and Fleck, N.A. *Metal Foams and Foam Metal Structures*. MIT Verlag, Bremen, 1999.
4. Asby, M.F., Evans, A., Fleck, N.A., Gibson, L.J., Hutchinson, J.W. and Wadley, H.N.G. *Metal Foam, A Design Guide*. Butterworth Heinmann, 2000.
5. Mancin, S., Zilio, C., Cavallini, A. and Rossetto, L. Pressure Drop During Air Flow in Aluminium Foams. *International Journal of Heat and Mass Transfer*, Vol. 53, 2010, pp.3121-3130.
6. Gibson, L. J and Asby, M. F. *Cellular Solid-Structures and Properties*. Cambridge Solid State Science Series, Cambridge University Press, 1997.
7. Zhao, Y.Y., Fung, T., Zhang, L.P. and Zhang, F.L. Lost Carbonate Sintering Process for Manufacturing Metal Foams. *Scripta Materiala*, Vol. 52, 2005, pp.295-298.
8. Goodall, R., Marmottant, A., Despoise, J.F., Salvo, L. and Mortensen, A. *Replicated Microcellular Aluminium With Spherical Pores*. Proceedings of Metfoam, Japan Institute of Metals, Sendai Japan, 2005.
9. Zhao, Y., Han, F. and Fung, T. Optimization of Compaction and Liquid State Sintering in The Sintering and Dissolution Process for Manufacturing Al Foams. *Materials Science Engineering*, Vol. 33, 2004, pp.117-125.
10. Yan, M.F. Solid State Sintering. In *Engineered Materials Handbook*, ASM International, Ohio, Vol. 4, 1991, p270-284.
11. Okuyama, K. *Powder Technology: Fundamentals of Particles, Particle Beds, and Particle Generation*. CRC Press, pp.213-218, 2006.
12. Rahaman, M.N. *Ceramic Processing and Sintering*. Marcel Dekker, 2nd Edition New York, 2003.
13. Richardson, D.W. *Modern Ceramic Engineering: Properties, Processing and Use in Design*. Marcel Dekker, 2nd Edition, New York, 1992.
14. German, R.M. Fundamentals of Sintering. In *Engineered Materials Handbook*, ASM International, Ohio, Vol. 4, 1991, pp.320-330.
15. Coble, R.L. Sintering of Crystalline Solid: Intermediate and Final State Diffusion Models. *Journal of Applied Physics*, Vol. 32, 1961, p787-792.
16. Ashby, M.F. and Swinkles, F.B. A Second Report on Sintering Diagrams. *Acta Metallurgica*, Vol. 29, 1981, pp.259-281.
17. Jinnapat, A. and Kennedy, A.R. The Manufacture of Spherical Salt Beads and Their Use as Dissolvable Templates for The Production of Cellular Solids Via Powder Metallurgy Route. *Journal of Alloys and Compounds*, Vol. 499, 2010, pp.43-47.
18. Suzuki, M. *Powder Technology Handbook*. Third Edition, CRC Press, 2006.
19. Rahaman, M.N. *Ceramic Processing and Sintering*. 2nd Edition, New York, Marcel Dekker, 2003, pp.723-733.